Steering Kinematics for a Center-Articulated Mobile Robot

Peter I. Corke and Peter Ridley

***Abstract*—This paper discusses the steering kinematics for a center-articulated mobile robot. Several models have been recently proposed in the literature and we use experimental data to compare and validate these models. The vehicle heading response to steering command is shown to include a dominant zero due a nonholonomic constraint, and this is verified by experiments conducted using a 30-t mobile vehicle at our laboratory. Simulation results are then used to show the significance of this zero and its effect on closed-loop heading angle control.**

***Index Terms*—Autonomous vehicle, load-haul-dump, nonholonomic, steering control.**

I. Introduction

Load-haul-dump (LHD) vehicles (see Fig. 1) transport ore in underground metaliferrous (noncoal) mines. Operation is cyclic, typically 15–18 trips/h, with round-trip travel distances from 100 to 600 m. The full or partial automation of underground truck haulage is considerably attractive to industry [1] since it has the potential to improve safety by removing people from the vehicles, while simultaneously increasing productivity. Automation of this type of vehicle has been reported by many groups including [2]–[4], and [5] provides a recent review.

The dynamics of the LHD are different to a normal free-steered vehicle such as a car or semi-trailer, which is commonly discussed in the literature. As observed by Altafini [6], the centre articulation gives the vehicle considerable maneuverability within the narrow confines of a tunnel. A number of papers [7]–[9] uses a simple 'bicycle-type' model for the LHD. Recently, DeSantis [10] and Altafini [11] have developed more complete models of the LHD, which include a nonholonomic constraint due to the articulation joint and the wheels.

The front and back sections of the vehicle are connected by a joint, H, with a vertical axis (see Fig. 2). The articulation angle is referred to as γ.

Two linear hydraulic cylinders acting in a push–pull configuration exert forces S and S' to actuate the joint (see Fig. 2). In addition to creating a moment about the pivot point, they exert lateral forces that are opposed by tire adhesion forces. In practice, the actuators are strong enough to break adhesion and scrape the wheels sideways across the ground when the vehicle is parked with brakes applied.

Section II introduces our notation and develops a steady-state model of the turning vehicle. This is extended in Section III to a full kinematic model which describes how the vehicle's pose evolves with time as a function of steering angle γ and ground speed v. This full model is compared experimentally with the simpler "bicycle" kinematic model and significant discrepancy is observed. Finally, in Section IV, the two models are compared in the context of a simple heading-angle control system.

We assume throughout that there is only point contact between wheel and ground, that the wheels do not slip, and that all motion is planar.

Manuscript received April 11, 2000; revised December 6, 2000. This paper was recommended for publication by Associate Editor E. Colgate and Editor A. De Luca upon evaluation of the reviewers' comments.

P. I. Corke is with CSIRO Manufacturing Science and Technology, Kenmore 4069, Australia (e-mail: pic@cat.csiro.au).

P. Ridley is with the School of Mechanical Engineering, Queensland University of Technology, Brisbane 4001, Australia.

Publisher Item Identifier S 1042-296X(01)04809-1.

Fig. 1. Picture of a typical LHD. This vehicle is around 4 m wide, 10 m long, weighs 28.5 t, and carries 8 t of ore.

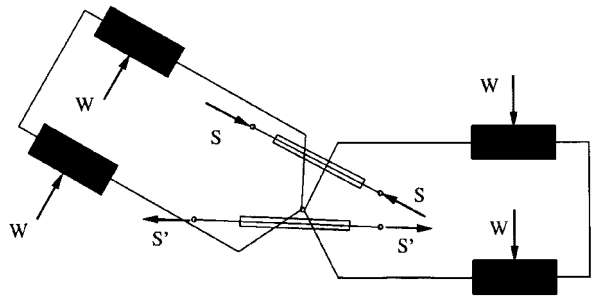

Fig. 2. Plan view of the LHD steering mechanism. W represents lateral forces due to tire adhesion and S and S' are the steering actuator forces.

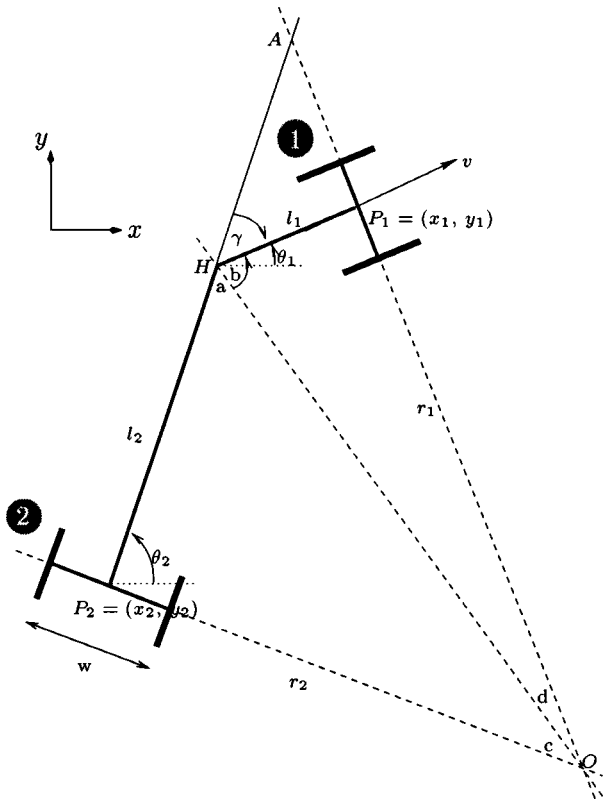

Fig. 3. Geometry of the LHD vehicle while turning. r_i is the distance from O to P_i.

II. Steady-State Turning

Fig. 3 shows the essential geometry of a centre articulated vehicle which we will use to develop a simple steady-state model for vehicle turning behavior, i.e., $\dot{\gamma} = 0$. We will also discuss the complications

1042–296X/01$10.00 © 2001 IEEE

introduced for a nonsymmetric vehicle, i.e., $l_1 \neq l_2$ (unlike [9] and [10]). For our particular LHD, $l_1 = 1.6$ m and $l_2 = 1.8$ m.

At the point H we can write

$$a + b + \gamma = 180^\circ \tag{1}$$

and for the right-angled triangles $\triangle OHP_1$ and $\triangle OHP_2$ we can write

$$d + b = 90^\circ \tag{2}$$

$$a + c = 90^\circ. \tag{3}$$

Substituting into (1) we determine that

$$c + d = \gamma. \tag{4}$$

Next, consider the right-angle triangle $\triangle OP_2A$, for which we can write

$$l_2 + \frac{l_1}{\cos\gamma} = r_2 \tan\gamma \tag{5}$$

$$\sin\gamma(r_1 + l_1 \tan\gamma) = l_2 + \frac{l_1}{\cos\gamma} \tag{6}$$

which can be simplified to yield the turning radii

$$r_1 = \frac{l_1 \cos\gamma + l_2}{\sin\gamma} \tag{7}$$

$$r_2 = \frac{l_2 \cos\gamma + l_1}{\sin\gamma}. \tag{8}$$

Interestingly, the two halves of the vehicle follow circles of different radii, and the ratio of radii of curvature

$$\frac{r_2}{r_1} = \frac{l_2 \cos\gamma + l_1}{l_1 \cos\gamma + l_2} \tag{9}$$

is identically equal to one only for the case $l_1 = l_2$ or $\gamma = 0$.

A consequence of this difference in radii is that the ground speed of the two vehicle halves is also different whilst turning. The vehicle has a separate differential for the front and rear wheels, each driven by the output of the gearbox. The input speed to the differential is the mean speed of its two associated wheels

$$\begin{aligned} \bar{\omega}_1 &= \frac{1}{2}\left(\Omega\left(r_1 + \frac{w}{2}\right) + \Omega\left(r_1 - \frac{w}{2}\right)\right) \\ \bar{\omega}_2 &= \frac{1}{2}\left(\Omega\left(r_2 + \frac{w}{2}\right) + \Omega\left(r_2 - \frac{w}{2}\right)\right) \end{aligned} \tag{10}$$

where w is the distance between wheels along the axle and Ω is the angular velocity of the vehicle moving along the circular arc. Combining (11) and (8), we can write the ratio of the mean front and back wheel speeds as

$$\frac{\bar{\omega}_2}{\bar{\omega}_1} = \frac{r_2}{r_1}, \qquad \Omega \neq 0 \tag{11}$$

which are equal only for the case of straight line motion, $\gamma = 0$, or turning with $l_1 = l_2$. For our vehicle, with a nonzero steer angle this effect is small, but the back wheels are required to rotate up to 2% faster than they are driven—effectively, the back will be dragged by the front leading to increased tire wear and stress on the articulation joint.

III. Full Kinematic Model

In this section, we will develop a general kinematic model of the vehicle that shows how heading angle evolves with time as a function of steering angle and velocity. DeSantis has recently proposed a dynamic model for the general n-trailer problem [12] and also for the specific center-articulated vehicle problem [10]. However, these dynamics models, like those of Hemami [13], have inputs of wheel and steering joint torques whereas the actual machine has inputs of angular velocities (motor RPM and steering cylinder flow rates), i.e., kinematic quantities. A further disadvantage of the dynamic model approach is that the inertial parameters are not known and would be difficult to estimate.

Instead we adopt the methodology of Altafini [11], which is summarized below. Referring to Fig. 3 we can write, for the first body

$$\dot{x}_1 = v\cos\theta_1 \tag{12}$$

$$\dot{y}_1 = v\sin\theta_1 \tag{13}$$

where v is the velocity of the vehicle. The relationship between P_1 and P_2 is given by

$$x_2 + l_2\cos\theta_2 + l_1\cos\theta_1 = x_1 \tag{14}$$

$$y_2 + l_2\sin\theta_2 + l_1\sin\theta_1 = y_1 \tag{15}$$

and we also know that

$$\theta_1 = \theta_2 - \gamma. \tag{16}$$

The constraint on rolling without slipping (nonholonomic constraint) implies that there can be no motion parallel to the axles, that is

$$\dot{x}_2\sin\theta_2 - \dot{y}_2\cos\theta_2 = 0 \tag{17}$$

$$\dot{x}_1\sin\theta_1 - \dot{y}_1\cos\theta_1 = 0. \tag{18}$$

Differentiating (14) and (15) with respect to time, substituting in (12), (13), (17), and (18), and then simplifying we can show that

$$\dot{\theta}_1 = -\frac{v\sin\gamma + l_2\dot{\gamma}}{l_1\cos\gamma + l_2}. \tag{19}$$

By comparison, the simple "bicycle" steering model of [9] predicts a yaw rate for the front of the vehicle of

$$\dot{\theta}_1 = -v\frac{\sin\gamma}{l_2 + l_1\cos\gamma} \tag{20}$$

which is similar to (19) but missing the $\dot{\gamma}$ term in the numerator. The bicycle model predicts that $\dot{\theta}_1$ is always zero at zero velocity, $v = 0$, but this is not observed in practice—articulating the vehicle while it is stationary, but with the brakes off, causes the front and back parts of the vehicle to rotate. The nonholonomic constraint of (19) is similar to the "slip model" of [9] but the dynamics are actually due to the assumed nonslip constraint.

Yaw rates for the front and back of the vehicle, respectively, $\Omega_f = \dot{\theta}_1$ and $\Omega_b = \dot{\theta}_2$, are related by

$$\Omega_f = \Omega_b - \dot{\gamma}. \tag{21}$$

All three variables can be measured on our experimental system. The front and back angular rates were measured by Crossbow IMU units (model DMU-6X on the front and model DMU-VG on the rear). Gyro bias was established and subtracted from the data before analysis. In forward motion, a positive hitch angle γ causes the vehicle to steer to the right. This is a negative yaw about the Z-axis which is upward.

Raw data from the experiment is shown in Fig. 4. Speed is constant at nearly 2 m/s. The steer angle is varying between approximately $\pm 20^\circ$ and the front and back have yaw rate varying between approximately $\pm 20^\circ$/s.

Yaw rate error, measured minus predicted, is compared in Fig. 5 for the two steering models. For the front of the vehicle the RMS errors are 5.0° and 2.3° for the bicycle and nonholonomic models, respectively. This would indicate that the nonholonomic constraint is significant to the vehicle's steering response even though the underlying assumption of no slip is likely to be violated in practice when driving over a rough dirt road.

We can rearrange (21) to form a residual from the measured quantities

$$\eta = \Omega_b - \Omega_f - \dot{\gamma}$$

which should be zero. Fig. 6 is a plot of η for this dataset which is essentially white noise (confirmed by autocorrelation measure) with superimposed impulses which we believe are due to slop and backlash in the articulation system. Note that this data was obtained while the

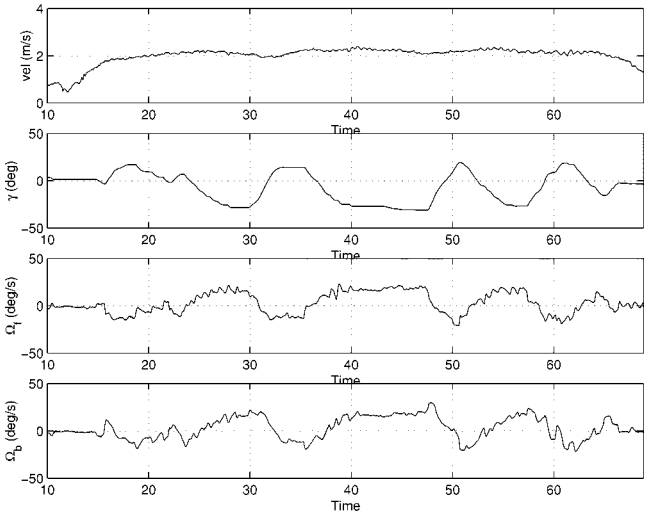

Fig. 4. Raw data from the trial.

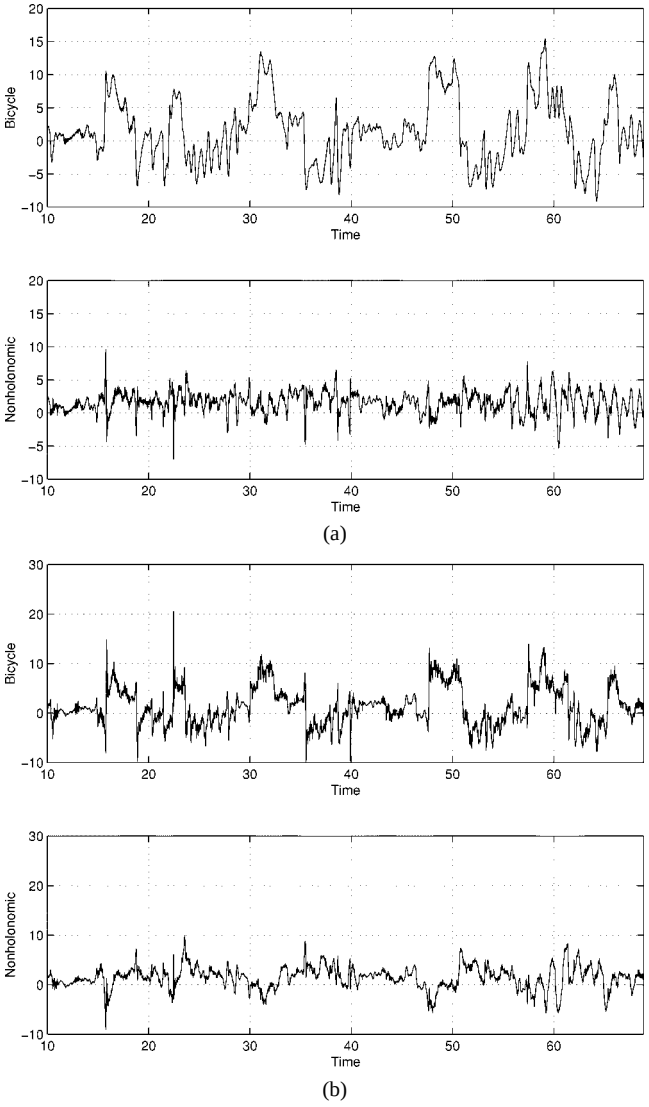

Fig. 5. Yaw rate prediction errors (°/s) for the two steering models. (a) Front. (b) Back.

vehicle was moving over uneven terrain and that vehicle/ground interaction forces act on the steering joint. It may be feasible to monitor the

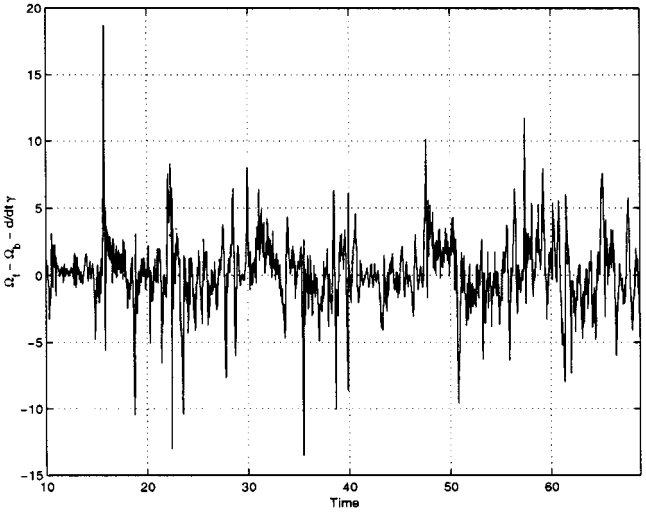

Fig. 6. Residual rotation $\Omega_f - \Omega_b - \dot{\gamma}$.

statistics of this residual online and use it to infer failure in sensors or actuators.

IV. Control Implications

In this section, we investigate the implication of the zero dynamics for the case of a simple linear heading controller, by comparing the performance with the bicycle and the full kinematic models.

As a first step we approximately linearize both models, by assuming that velocity v is constant and $\gamma \approx 0$

$$\left(\frac{\Theta(s)}{\Gamma(s)}\right)_{\text{bicycle}} = \frac{v}{s(l_1+l_2)} \tag{22}$$

$$\left(\frac{\Theta(s)}{\Gamma(s)}\right)_{\text{exact}} = \frac{sl_2+v}{s(l_1+l_2)} \tag{23}$$

where Θ and Γ are the Laplace transforms of θ and γ, respectively. Both models include the forward velocity as a gain in the numerator, but the exact model has a zero at $s = -v/l_2$. This zero is always within the left-hand half plane except at zero speed when it is at $s = 0$ and acts as a pure differentiator. At low speeds, say 5 km/h, and for our vehicle dimensions the zero is dominant at 0.77 rad/s.

If the input rate and saturation limits are ignored, then a simple high-gain proportional controller is effective for heading control. We choose to make the loop gain invariant to velocity by choosing the controller gain

$$K' = \frac{K}{|v| + \delta}$$

where K is the adjustable gain parameter and δ is a small value to avoid singularity. Fig. 7 shows the simulated response of both models, and we can see that the bicycle plant model has zero error for constant heading demand (as expected for a Type I plant). The exact model has a slower error ramp and decay due to the action of the dominant zero. To achieve improved dynamic performance at low speed, this zero must be dealt with explicitly in the control design, possibly by introducing a feedforward term. As vehicle speed increases, the zero dynamics are seen to decay more quickly, and at high speed, the vehicle more closely approximates a bicycle, and a controller based on the incomplete bicycle model will perform adequately on the exact plant model.

V. Conclusions

The vehicle's response to steering demand has been shown, theoretically and experimentally, to contain a speed-dependent zero term due

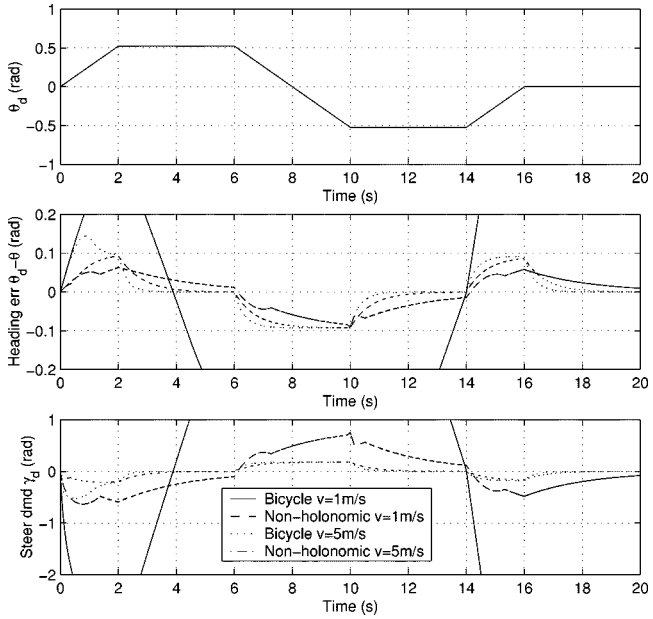

Fig. 7. Simulated steering response for bicycle and nonholonomic models for plant with no rate or saturation limits and $K = 10$ and for two speeds $v = 1, 5$ m/s.

to a nonholonomic constraint. The bicycle and exact models were then compared in the context of a heading control loop where the effect of the zero on error and input demand is quite marked, particularly at low speed. As vehicle speed increases, the kinematics tend toward those of a bicycle. However, at low speed, such as required when turning tight corners, the difference is significant and given the confined environment must be taken into account.

ACKNOWLEDGMENT

The first author would like to thank C. Altafini, KTH Stockholm, for discussions on this topic. Experimental data was provided by AMIRA sponsored project P517 and the CSIRO LHD project team: G. Winstanley, J. Roberts, E. Duff, P. Sikka, L. Overs, S. Wolfe, R. McCasker, and J. Cunningham.

REFERENCES

[1] J. Cunningham, P. Corke, H. Durrant-Whyte, and M. Dalziel, "Automated LHD's and underground haulage trucks," *Australian Journal of Mining*, 1999.

[2] L. Bloomquist and J. P. Huissoon. (1996) Navigation system for autonomous underground mining vehicles. [Online]. Available: http://sail.uwaterloo.ca/ labloomq/workshop/info.html

[3] J. D. Lane, "Automatic steering system for an underground mine haul truck," Master's, Colorado School of Mines, 1992.

[4] G. Eriksson and A. Kitok, "Automatic loading and dumping using vehicle guidance in a Swedish mine," in *International Symposium on Mine Mechanization and Automation*, Colorado, June 1991, pp. 15.33–15.40.

[5] J. Roberts and P. Corke, "Automation of underground truck haulage," in *International Symposium on Mine Mechanization and Automation*, Brisbane, July 1997, pp. b5.23–32.

[6] C. Altafini, "Why to use an articulated vehicle in underground mining operations?," in *Proc. IEEE Int. Conf. Robotics and Automation*, May 1999, pp. 3020–3025.

[7] J. Steele, C. Ganesh, and A. Kleve, "Control and scale model simulation of sensor-guided LHD mining machines," *IEEE Trans. Industry Applications*, vol. 29, Nov 1993.

[8] A. Hemami and V. Polotski, "Path tracking control problem formulation of an lhd loader," *Int. J. Robot. Res.*, vol. 17, pp. 193–198, Feb 1998.

[9] S. Scheding, G. Dissanyake, and E. M. N. H. Durrant-Whyte, "An experiment in autonomous navigation of an underground mining vehicle," *IEEE Trans. Robot. Autom.*, vol. 15, pp. 85–95, Feb 1999.

[10] R. DeSantis, "Modeling and path-tracking for a load-haul-dump mining vehicle," *Journal of Dynamic Systems, Measurement and Control*, vol. 119, pp. 40–47, Mar 1997.

[11] C. Altafini, "A path-tracking criterion for an lhd articulated vehicle," *Int. J. Robotics Research*, vol. 18, pp. 435–441, May 1999.

[12] P. Bolzern, R. DeSantis, A. Locatelli, and S. Togno, "Dynamic model of a two-trailer articulated vehicle subject to nonholonomic constraints," *Robotica*, vol. 14, pp. 445–450, 1996.

[13] A. Hemami and V. Polotski, "Dynamics of a dual-unit articulated vehicle for path tracking control problem formulation," in *Proc. Int. Conf. Control Applications*, Hartford, CT, Oct 1997, pp. 173–176.

Payload Maximization for Open Chained Manipulators: Finding Weightlifting Motions for a Puma 762 Robot

Chia-Yu E. Wang, Wojciech K. Timoszyk, and James E. Bobrow

***Abstract*—Although the dynamic equations of motion of open-chained robot systems are well known, they are seldom taken into account during the planning of motions. In this work, we show that the dynamics of a robot can be used to produce motions that extend the payload capability beyond the limit set by traditional methods. In particular, we develop a point-to-point weightlifting motion planner for open-chained robots. The governing optimal control problem is converted into a direct, SQP parameter optimization in which the gradient is determined analytically. The joint trajectories are defined by B-spline polynomials along with a time-scale factor. The algorithm is applied to a Puma 762 robot, with its physical limitations incorporated into the formulation. The torque limits are formulated as soft constraints added into the objective function while the position and velocity limits are formulated as hard, linear inequality constraints, on the parameters. The solutions obtained with our algorithm extend the robot's payload capability while reducing the joint torques. Interestingly, nearly all the trajectories found pass through singular configurations, where large internal forces from the robot are applied to the payload and little torque is needed from the motors. A video file of the resulting motions can be found at http://www.eng.uci.edu/~chwang/project/puma762.html.**

***Index Terms*—B-spline, dynamic motion planning, open chained manipulator, optimal robot control, optimization.**

I. INTRODUCTION

The majority of current robot motion planning algorithms, such as those found in well-known texts (see, e.g., [10]), ignore the dynamics of the robot during the motion planning phase. In this paper, we show how the dynamics of a manipulator can be used to extend its payload capability beyond the limits established by the manufacturer. The goal of the research was to develop an algorithm that maximizes the robot payload while taking into account realistic constraints such as joint torque limits and velocity bounds. Our solutions also minimize joint torques

Manuscript received August 7, 2000. This paper was recommended for publication by Associate Editor I. Walker and Editor A. De Luca upon evaluation of the reviewers' comments. The work was supported by the National Science Foundation under Grant IIR-9711782. This paper was presented in part at the IEEE International Conference on Robotics and Automation, Detroit, MI, May 1999.

The authors are with the Department of Mechanical and Aerospace Engineering, University of California, Irvine, CA 92697 USA (e-mail: chwang@eng.uci.edu; wtimoszy@eng.uci.edu; bobrow@eng.uci.edu).

Publisher Item Identifier S 1042-296X(01)04813-3.

1042–296X/01$10.00 © 2001 IEEE